

A Control Strategy of Photovoltaic Hybrid Energy Storage System Based on Adaptive Wavelet Packet Decomposition

Wanlu Zhu, Ye Yang, Pengfei Zhi*, Zhengzhuo Liang

Department of Automation, Jiangsu University of Science and Technology, Zhenjiang 212000

*E-mail: zhipengfei@just.edu.cn

Received: 23 August 2022 / Accepted: 22 September 2022 / Published: 10 October 2022

This paper analyzes the output power fluctuation characteristics of a photoelectric field based on the frequency domain. It also proposes a photoelectric power allocation method based on adaptive wavelet packet frequency dividing. This method provides reasonable distribution of low-, intermediate- and high-frequency energy among the different energy storage elements. By combining the energy storage characteristics of supercapacitors and lithium batteries, a coordinated control strategy of SC-Li batteries is designed to effectively suppress the impact of photovoltaic power fluctuations on the grid. Compared with the original power of photovoltaics, the method proposed herein greatly reduces the fluctuation of photovoltaic power, thereby allowing the final grid-connected power area to smooth, which leads to stable and safe development of power grids and energy storage components. Finally, a semi-physical simulation of the measured data of a certain photoelectric field verifies the effectiveness of the method.

Keywords: Hybrid energy storage; Coordinated control strategy; Adaptive wavelet packet decomposition

1. INTRODUCTION

In 2021, China increased its new energy power generation capacity to 1.12 gigawatts, accounting for 47.1% of the country's total installed capacity. With its unique advantages, photovoltaic power generation has attracted the attention of experts and scholars worldwide[1]. In the regional microgrid, improving the power utilization rate of photovoltaic power generation can indirectly reduce the dependence of the microgrid on external power while reducing the cost of transportation[2, 3]. And many countries have introduced PV subsidy policies to promote the development of the PV industry, making the cost of PV power generation continue to fall. Despite these advances, photovoltaic electricity has unstable and uncontrollable characteristics. In some regional microgrids, the internal energy storage system is combined with external power distribution systems to complete the power

supply to the regional load[4, 5]. Long-term absorption of the unstable photovoltaic electricity by the microgrid energy storage system decreases the lifetime of the lithium battery[6-9].

Recently, scholars have used hybrid energy storage active power distribution combined with hybrid energy storage control strategies to smooth the power fluctuations of photovoltaic and wind power generation. In terms of active power allocation of mixed energy storage, empirical mode decomposition (EMD) was used to realize the distribution of active power, but the noise in the EMD decomposition process was relatively large and was prone to modal aliasing [10]. In [11, 12], the authors proposed a hybrid energy storage power distribution strategy based on wavelet packet decomposition. The power signal was decomposed into high, medium, and low frequency parts through wavelet packet analysis, and power reconfiguration. However, there was a large delay between the target power and the generation output power. A hierarchical model predictive control dynamic active power allocation strategy is proposed in [13], which was verified via PSCAD simulation. This hierarchical model has high requirements for the current SOC calculation accuracy. Regarding the smooth output fluctuation control strategy of photovoltaic hybrid energy storage, model predictive control was used to improve the accuracy of photovoltaic output prediction to obtain the best energy storage reference power and reduce the smooth output fluctuation [14]. However, wavelet transform has poor frequency resolution in high frequencies and poor time resolution in low frequencies. A strategy for maximum power tracking and hybrid energy storage was proposed in [15] to balance photovoltaic power fluctuations in coordination. In this paper, the optimization goal of annual net income maximization has limitations. In order to smooth solar power fluctuations, Atif introduced the use of Savitzky-Golay filters to reduce battery charge and discharge power. The simulation results show the properties of the smoothness filter and compare its performance against low pass filtering (LPF), moving average (MA) filtering, Gaussian filter (GF)[16].

This article aims to reduce the fluctuation of photovoltaic power generation and ensure a stable and safe grid-connected voltage. Due to the fluctuation characteristics of photoelectric power under different photoelectric output scenarios, the paper proposes an adaptive wavelet decomposition method that smooths the fluctuation of photoelectric power in combination with the grid-connected fluctuation standard of photoelectricity. It also realizes the general applicability of the decomposition algorithm. The innovation of this paper lies in the design of a coordinated control strategy for multiple supercapacitors to work alternately in view of the low energy storage of a single supercapacitor to improve the efficiency of smoothing power fluctuations.

2. CONTROL STRATEGY RESEARCH

2.1. System structure

The output power fluctuation components of the photovoltaic electricity generation in the microgrid are very complex and irregular. In the hybrid energy storage system structure using photovoltaic power generation, this article mainly considers the relationship between the following powers in the system:

$$P_v = P_0 + P_{Li} + P_{sc} \tag{1}$$

$$P_{HESS} = P_{sc} + P_{Li} \tag{2}$$

$$P_{HESS}^* = P_{sc}^* + P_{Li}^* \tag{3}$$

$$P_v^* = P_{HESS}^* + P_0 \tag{4}$$

where P_v —total output power of photovoltaics; P_{HESS} —input power of hybrid energy storage system; P_{HESS}^* —output power of the hybrid energy storage system; P_0 —direct grid-connected power of photovoltaic power generation; P_{sc} —input power of supercapacitor unit; P_{Li} —direct input power of lithium battery; P_v^* —actual photovoltaic grid-connected power.

Figure 1 shows the power distribution structure of the hybrid energy storage system designed herein.

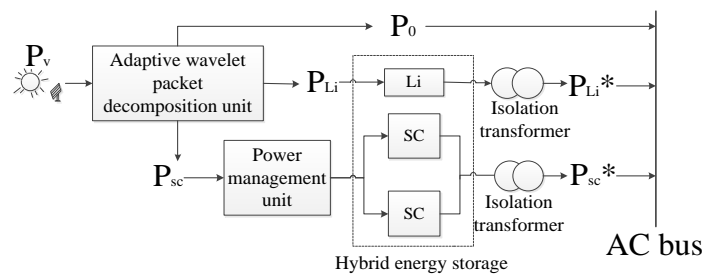


Figure 1. System power allocation diagram

2.2. Optical power allocation method based on adaptive wavelet packet decomposition

The wavelet packets can decompose both high-frequency signal and low-frequency signal. The wavelet packet decomposition diagram of the original signal is shown in Figure 2.

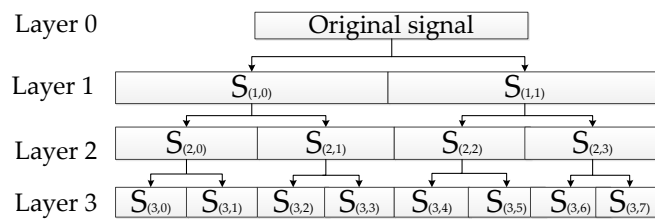


Figure 2. Schematic diagram of the wavelet packet decomposition method

In actual operation, the photovoltaic power generation is obtained through real-time sampling. The conventional wavelet packet decomposition method limitation is that it can only process current power and historical power signals[17]. This leads to a large delay between target power and photovoltaic delivered power. Therefore, the target power obtained after conventional wavelet packet decomposition is defective, and it cannot reflect the trend of photovoltaic power generation accurately [18].

To reduce the delay, the paper presents an improved adaptive wavelet packet decomposition method. When the photovoltaic output power is relatively stable, the number of wavelet packet decomposition layers ought to be reduced. When the photovoltaic output power changes drastically, the number of wavelet decomposition layers increases, and then the adaptive wavelet packet decomposition unit extracts the low-frequency components of photovoltaic power generation as the smoothing target. We propose an adaptive wavelet packet decomposition method based on the above ideas, with the number of decomposition layers being determined by the degree of grid power fluctuation resulting from the change of photovoltaic output power.

First, n -layer wavelet packet decomposition is performed on the photovoltaic output power signal to reconstruct the signal in the $S_{(n,0)}$ frequency band. Then, the root mean square difference ΔP_n between the photovoltaic output signal $P(t)$ and the $S_{(n,0)}$ frequency band signal can be calculated as shown in the following equation:

$$\Delta P_n = \sqrt{\frac{\sum (P(t) - P_{(n,0)})^2}{T}} \tag{5}$$

with T —signal time length.

Combining ΔP_n with the present photovoltaic power-output signal and bandwidth, the power fluctuation of the grid can be calculated, and the wavelet packet decomposition layer number n can now be selected according to the fluctuation of the grid voltage, as shown in the following equation:

$$n = \begin{cases} 5, d < 1\% \\ 6, 1\% \leq d < 2\% \\ 7, 2\% \leq d < 5\% \\ 8, d \geq 5\% \end{cases} \tag{6}$$

with d —grid voltage fluctuation range.

According to the performance differences of energy storage equipment, an adaptive wavelet packet is used to divide the frequency of the photoelectric power into high, intermediate, and low frequencies. Since the low frequency signal has large energy and relatively stable fluctuations, it is directly connected to the grid. Energy-based energy storage equipment can smoothly process power signals with large amplitude and low frequency. Thus, intermediate-frequency signals with relatively stable power fluctuations are allocated to large-capacity energy storage lithium batteries. Finally, the high-frequency signal with a fast fluctuation speed is allocated to the supercapacitor.

The db6 wavelet is used to decompose the total photoelectric output P_v into seven layers, where P_{h0} is the low-frequency signal, P_{h1} and P_{h2} are the intermediate frequency signals, and P_{h3} – P_{h127} are the high-frequency signals. The photovoltaic power distribution can be calculated as follows:

$$P_v = P_{h0} + P_{h1} + P_{h2} + \dots + P_{h127} \tag{7}$$

$$P_0 = P_{h0} \tag{8}$$

$$P_{Li} = P_{h1} + P_{h2} \tag{9}$$

$$P_{sc} = P_{h3} + P_{h4} + P_{h5} + \dots + P_{h127} \tag{10}$$

2.3. Charging and discharging status of the hybrid energy storage system

The power management unit sets the charging and discharging state by analyzing the direct grid-connected power of photovoltaic generation in the microgrid and the direct grid-connected power of regional loads.

First, the paper sets charging threshold power of the mixed energy storage system. After the original photoelectric power signal is decomposed into high, intermediate, and low frequencies by the adaptive wavelet packet, the power management unit determines the relationship between the high-frequency power in the original photoelectric power signal and the set charging threshold power. When the high-frequency power is greater than the charging threshold power, the supercapacitor unit in the mixed energy storage system absorbs the high-frequency power in the original photoelectric power signal, while the supercapacitor unit is in the charging state. When the high-frequency power is lower than the charging threshold power, the hybrid energy storage system does not operate. In addition, when the intermediate-frequency power in the original photoelectric power signal is directly output to the lithium battery in the hybrid energy storage system, the hybrid energy storage system is also in the charging state.

The discharging state of the hybrid energy storage system depends on the low-frequency signal of the original photoelectric power signal because the low-frequency energy is significantly larger than the intermediate frequency and high frequency energy. When the low frequency power cannot meet the power demand of the regional load, the hybrid energy storage system then releases the electric energy stored in the lithium battery to supplement the insufficient power, meaning the battery is in the discharging state. When the low-frequency signal of the original photoelectric power signal meets the regional load power, the hybrid energy storage system does not need to supplement power; thus, the excess power in the low-frequency power is absorbed and stored in the lithium battery (i.e., the battery is in the charging state). The charge-discharge states of the mixed energy storage system are composed of the charge-discharge states of the supercapacitor and the lithium battery.

2.4. Coordinated control strategy of super capacitor-lithium battery

To ensure high efficiency and smooth photoelectric fluctuations, we first propose a criterion for judging the completion of supercapacitor charging and discharging, and the charging and discharging states of supercapacitors are switched by relying on this criterion. In addition, we design a control strategy for switching the charge-discharge of multiple supercapacitors by taking advantage of the rapid charging and discharging of supercapacitors. After analyzing the characteristics of fast charge-discharge of supercapacitors, we design a coordinated control strategy for switching the charge-discharge of multiple supercapacitors.

Figure 3 shows the configuration of the SC-Li-SC hybrid energy storage system proposed herein. We use the solid line to represent the power, and the dotted line to represent the feedback signal; SC_A and SC_B represent supercapacitor A and supercapacitor B, respectively; Li is the lithium battery; and A1, A2, A3, and A4 correspond to ammeter 1, ammeter 2, ammeter 3, and ammeter 4, respectively. Under this control strategy, the charging and discharging completed are the two critical

states of supercapacitor A and supercapacitor B. In order to express it more clearly, the following table lists the four states of the supercapacitor A and B corresponding to the four formulas.

Table 1. The state of super capacitor.

Formula	State
$SOC_A = max_A$	supercapacitor A is in the charging completed state
$SOC_A = min_A$	supercapacitor A is in the discharging completed state
$SOC_B = max_B$	supercapacitor B is in the charging completed state
$SOC_B = min_B$	supercapacitor B is in the discharging completed state

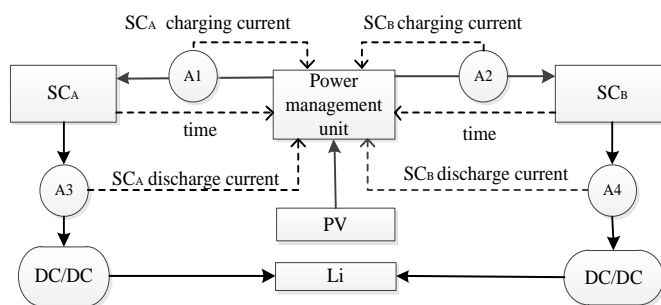


Figure 3. Structure diagram of the SC-Li-SC photovoltaic power suppression device used herein.

The charging time of the supercapacitor unit is affected by the intensity of the regional light energy, and because of the difficulty in accurately reading the state of charge (SOC) of the supercapacitor, according to the SOC of the super capacitor, there are technical difficulties in judging accurately whether the supercapacitor is fully charged and discharged [19].

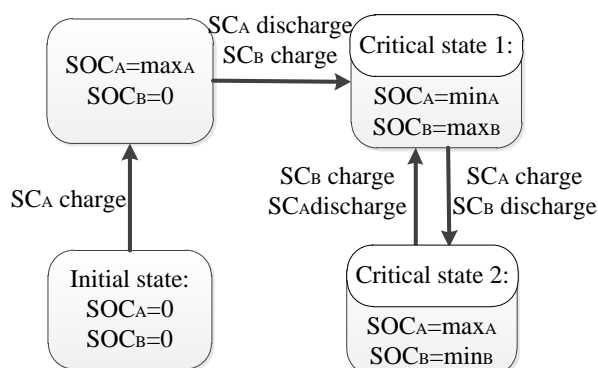


Figure 4. State transition of a supercapacitor unit.

To make sure of high veracity of the control strategy, we used a method for detecting the charging and discharging current to judge the charge and discharge status of the supercapacitor. When photoelectric are charging the supercapacitor, if the current gradually tends to 0 and the terminal

voltage no longer rises, the supercapacitor is considered to be fully charged (i.e., the supercapacitor moves from the initial SOC, $SOC = min$, to the end SOC, $SOC = max$). During the discharging process of the supercapacitor, if the current gradually tends to 0 and the terminal voltage no longer drops, the supercapacitor is considered discharged. The supercapacitor has dropped from the terminal SOC, ($SOC = max$) to the initial SOC ($SOC = min$)

Figure 4 shows the state transition of the supercapacitor unit.

After initial status, the power management unit controls the photoelectric to charge the supercapacitor A. The power management unit operates in critical condition 1 first and then in critical condition 2. Critical condition 1 indicates that the terminal voltage of supercapacitor B no longer rises. At this point, charging current detected by current sensor A2 tends to 0, supercapacitor B is fully charged, and current sensor A3 detects that the discharge current of supercapacitor A tends to 0. The operation performed by the power management unit at this point is to switch supercapacitor A to charge and supercapacitor B to discharge. Critical condition 2 indicates that the terminal voltage of supercapacitor A no longer rises. At this point, the charging current detected by current sensor A1 tends to 0, supercapacitor A has been fully charged, and current sensor A4 detects that the discharge current of supercapacitor B tends to 0. The operation performed by the power management unit at this point is to switch supercapacitor B to charge and supercapacitor A to discharge. The whole process of coordinated control is shown in Fig. 5.

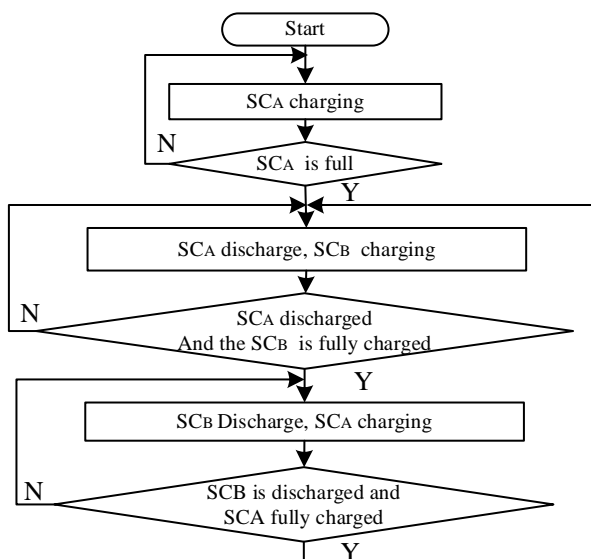


Figure 5. Coordinated control process.

The charging time of supercapacitor A (i.e., from the start of charging until the terminal voltage of supercapacitor A no longer rises and the charging current detected by current sensor A1 tends to 0) is T_{Ac} . The charging time of supercapacitor B (i.e., from the start of charging until the terminal voltage of supercapacitor B no longer rises and the charging current detected by current sensor A2 tends to 0) is T_{Bc} . The discharging times of supercapacitors A and B after being stabilized by the isolating

transformer voltage stabilizing device (when the discharge current reaches 0 and the terminal voltage is too low to meet the demand for continuing to charge the lithium battery) are both T_d .

The constraint condition of the control strategy is time, and the corresponding decision is made based on the time change of the control system. For the convenience of expression, let:

$$T_0 = T_{AC} \tag{11}$$

$$T_1 = \max\{(T_0 + T_d), (T_0 + T_{BC})\} \tag{12}$$

$$T_2 = \max\{(T_1 + T_0), (T_1 + T_d)\} \tag{13}$$

$$T_k = \begin{cases} \max\{(T_{k-1} + T_d), (T_{k-1} + T_{BC})\}, & k \text{ is an odd number} \\ \max\{(T_{k-1} + T_0), (T_{k-1} + T_d)\}, & k \text{ is an even number} \end{cases} \tag{14}$$

The power management unit detects the change of time t , corresponding to the state transition of the super capacitor unit. The control strategies made at different times are shown in the following table.

Table 2. Control strategies of different times.

	Power management unit action	Time constraint	Supercapacitor working status
Stage 1	Keep SC_A charged and SC_B not working	$t < T_0$	SC_A is charging and SC_B is not working
Critical state 1	Switch SC_A to discharge and SC_B to charge	$t = T_0$	
Stage 2	Keep SC_A discharged and SC_B charged	$T_0 < t < T_1$	SC_A is discharging and SC_B is charging
Critical state 2	Switch SC_A to charge and SC_B to discharge	$t = T_1$	
Stage 3	Keep SC_A charged and SC_B discharged	$T_1 < t < T_2$	SC_A is charging and SC_B is discharging

3. CHARACTERISTIC ANALYSIS AND MODEL STUDY OF SUPERCAPACITORS AND LITHIUM BATTERIES

At present, common energy storage devices can be divided into power-usage energy storage devices and energy- usage energy storage devices according to their energy storage characteristics. In this paper, we analyze the characteristics of the supercapacitor as a power- usage energy storage device and the large-capacity energy storage lithium battery as an energy-usage energy storage device, and provide a model basis for the simulation analysis.

3.1 Characteristic analysis and equivalent model for the supercapacitor

Supercapacitors have higher power density and cycle stability than lithium batteries [20]. Depending on the complexity of the model and the actual application scenarios, the common supercapacitor modeling is divided into the following categories: series RC equivalent model,

modified series RC equivalent model, linear RC network model, and nonlinear RC network model [21-24]. Among them, the series RC equivalent model has a simple structure compared with the other three models, and the circuit structure only consists of capacitors and resistors in series, which characterizes the transient dynamic effects of supercapacitors, and therefore cannot be used in complex energy storage systems while facilitating the calculation of circuit parameters for charging and discharging processes [25, 26]. The improved series RC equivalent model is improved by not only characterizing the transient dynamic effects of the supercapacitor, but also by considering the leakage current effect, which is realized in the circuit structure by connecting a resistor in parallel with the capacitor of the series RC equivalent circuit. Since the leakage current effect of the supercapacitor cannot really be avoided in some scenarios, the improved series RC equivalent circuit model contributes to the accuracy of the supercapacitor modeling. The linear RC network model and the nonlinear RC network model are designed to reflect the large-area porous supercapacitor, and both have the problem of difficult model parameter identification due to their high model complexity. The leakage current effect, which is not considered in the linear RC network model, is realized in the nonlinear RC network model, which consists of transient branches, long-term branches, delayed branches, and resistors characterizing the leakage current effect in parallel, and this model largely reflects the physical characteristics of the supercapacitor.

The supercapacitor is proposed herein to cope with frequent charging and discharging, which needs to focus on its dynamic response characteristics, and there is no energy loss due to self-discharge after charging is completed, i.e. leakage current effect. So there is no need to improve the shunt resistance in the series RC circuit. Therefore, we use the series RC equivalent circuit as the super capacitor simulation model, as shown in Figure 6.

According to circuit knowledge, the mathematical relationship between the supercapacitor terminal voltage U_c and the charge and discharge current I_c in the model can be obtained as follows:

$$U = IR + \frac{\int I dt}{C} \quad (15)$$

Assuming that the normal working voltage range of the supercapacitor is (U_{min}, U_{max}) , the energy stored by the supercapacitor can be calculated as:

$$W_c = \frac{C(U_{max}^2 - U_{min}^2)}{2} \quad (16)$$

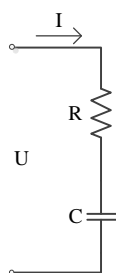


Figure 6. Supercapacitor series RC model used herein.

In the herein designed hybrid energy storage system, supercapacitors are used as high-frequency power smoothing device and require real-time dynamic response performance. They work in voltage outer loops and current inner loops. The control strategy block diagram for this system is shown in Figure 7. For the control of the supercapacitor, the outer loop is a voltage loop, and the bus voltage is first guaranteed to be stable while ensuring that the photovoltaic voltage does not exceed the withstand voltage limit of a single supercapacitor. The voltage outer loop ensures control accuracy, namely, the DC side bus voltage can be stabilized through the integration of the PI controller.

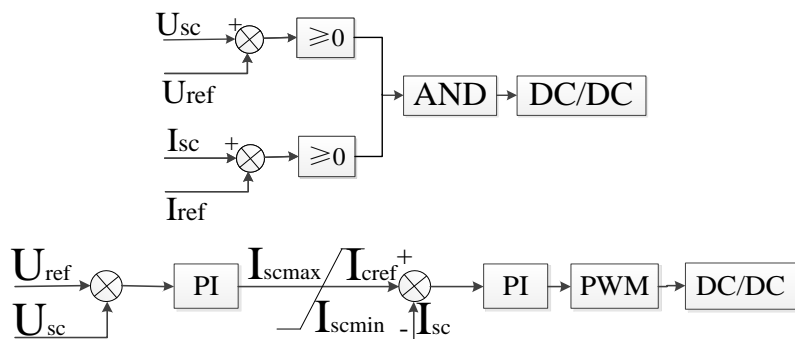


Figure 7. Supercapacitor control strategy used herein.

3.2 Lithium battery characteristic analysis and equivalent model

Lithium batteries have the advantages of high output power per unit volume, no memory and fast charging and discharging [27]. Currently Thevenin and Rint models are commonly used in the study of lithium batteries. Thevenin model is a simulation model designed by analogizing the properties of a battery with a capacitor. It can accurately reflect the dynamic characteristics of lithium batteries under different operating conditions, but has the disadvantage of complex and difficult parameter identification due to the multiple resistors and capacitors involved [28]. In this paper, the battery is used only as a general energy storage element, thus the Rint model is used, which can eliminate the need to consider the polarization characteristics of the lithium battery and having the advantage of a simple modelling approach.

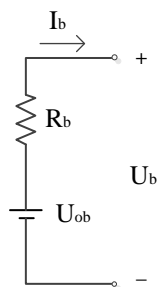


Figure 8. Rint model of the lithium battery used herein.

Figure 8 shows the Rint model of the lithium battery used in the simulation. Combining the above coordinated control strategy, the working status of the lithium battery can be obtained. Thus, according to the relationship between the photovoltaic power and the power required by the regional load to absorb or release electrical energy, it is only regarded as a general use of energy storage components without considering the polarization property of the lithium battery.

In this model, U_b is the terminal voltage of the lithium battery, I_b is the current flowing into the battery, the voltage source U_{ob} and the internal resistance R_b are variables, and their values depend on the SOC, temperature, and charge-discharge rate of the battery. This model only needs to determine the two parameters of battery open circuit voltage and internal resistance. The model thus ignores the polarization characteristics. To some extent, it reflects the dynamic performance of the lithium battery. According to Ohm's law:

$$U_b = U_{ob} - I_b R_b \tag{17}$$

When the influence of temperature on the internal resistance is not considered, R_b can be obtained by the following formula:

$$R_b = \frac{R_0}{\left(1 - \frac{C}{C_{0.1}}\right)^K} \tag{18}$$

where R_0 —internal resistance of the battery when fully charged; $C_{0.1}$ —maximum amount of electricity the battery can discharge when discharged at a rate of 0.1 C; C —power released from a lithium battery; and K —coefficient related to the discharge rate.

The lithium battery can operate in electric energy storage and electric energy compensation mode. When the power generated by the photovoltaic installation is below the load power supply, the large-capacity lithium battery operates in the energy compensation mode, and the output rated power value is used in conjunction with limited photovoltaic power generation to meet the load power. When the large-capacity lithium battery operates in the energy storage mode, the control method is similar to that used for the supercapacitor. The block diagram of the control strategy for a large-capacity lithium battery is shown in Figure 9.

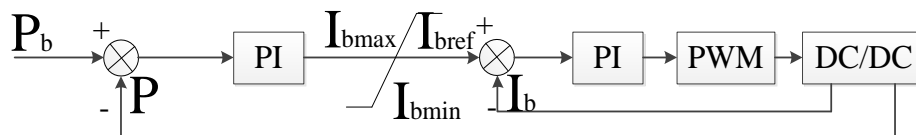


Figure 9. Lithium battery control strategy used herein.

4. SIMULATION ANALYSIS

4.1. Semi-physical simulation platform

Semi-physical simulation technology combines common offline simulation software and low-power physical simulation advantages, making it easy to change the topology and simulate fault

conditions. For the research of power grids and microgrids, because the physical simulation system is very complex, mathematical modeling is difficult, and accurate modeling is impossible. In addition, physical simulation is affected by the hardware equipment, environment, and other factors; the cost is high; and it is not easy to simulate the conditions with strict constraints. Placing the physical system in the computer environment for simulation can thus solve the above problems and can integrate the advantages of the above two methods [29].

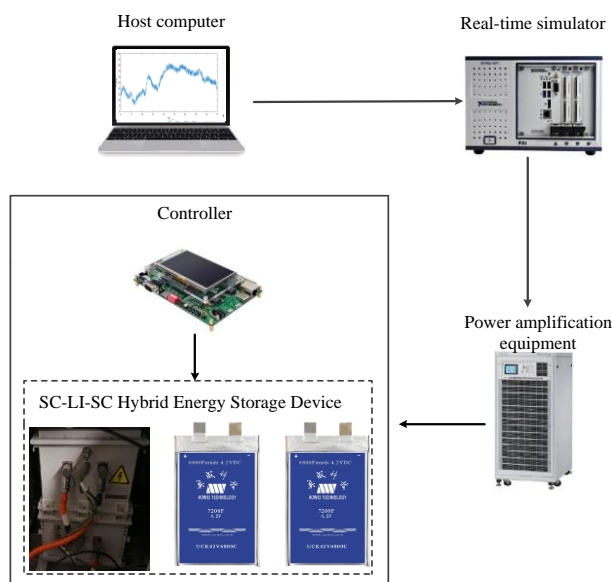


Figure 10. Hardware-in-the-loop simulation platform construction.

The typical capacity of photovoltaic power plants is in the range of megawatts. With the technological advancement of power amplification equipment, the supported power and response speed have been continuously improved. In this sense, power amplification equipment can be combined with power real-time simulators to test power electronic devices. Combined with the structure diagram of the hybrid energy storage photoelectric smoothing component, the configuration of the hybrid energy storage device semi-physical simulation platform designed herein is shown in Figure 10. The supercapacitor is Aowei Technology's UCK42V6800C, and the most relevant parameters of this device are shown in Table 3. The lithium battery selected in this article is produced by AVIC Lithium Battery. The monomer parameters are showed in Table 4.

Table 3. Parameters of the UCK42V6800C unit.

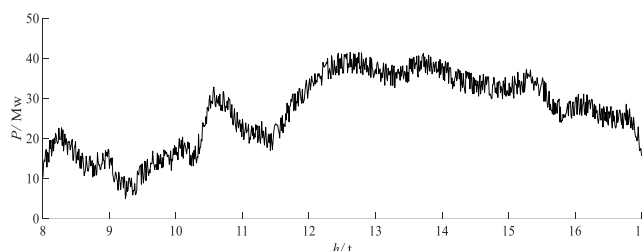
Operating voltage (V)	2.8–4.0
Nominal capacity (F)	7200
Energy storage capacity (W·h)	8.5
Energy density (W·h/kg)	71
Standard charge-discharge current (A)	20
Maximum charge-discharge current < 20 s (A)	45

Table 4. Parameters of the lithium battery.

Nominal voltage (V)	3.3
Nominal capacity (Ah)	60
Energy storage capacity (W·h)	198
Quality (kg)	2.5
Volume (L)	1.15

4.2. Example analysis

In the simulation process, we set the regional photovoltaic power generation of a microgrid to be 8–17h as the research object. The simulation data were sourced from Shandong Jinan Linuo Sunshine Science and Technology Park. The equipped capacitor of the photovoltaic power plant was 50MW, the sampling period was 36 s, and the charging threshold power of the energy storage system was set to 0.8 MW. The photovoltaic power generation P_v in the area was collected, and the power change diagram is shown in Figure 11.

**Figure 11.** Power change curve obtained within 8–17 h.

According to the original sampled data, the maximum power fluctuation of the hybrid energy storage device before smoothing reached 4.86 MW, while the average power fluctuation of the entire cycle was 3.56 MW.

According to the Chinese national standard "Technical Regulations for Connecting Photovoltaic Power Stations to Power Systems" (GB/T 19964-2012), the rate of change of active power in photovoltaic plans should not exceed 10% of the installed capacity/min. Combining the sample data and Equation (6), the maximum power fluctuation per minute should not be greater than 0.5 MW, and the number of decomposition layers is 8. The measurement time is 9 h, with a total of $N = 900$ sampling points.

In order to select the dividing time between the charging and discharging response of the lithium battery and the supercapacitor, 200 charging and discharging experiments were conducted on the supercapacitor and lithium battery respectively. The experiment processes all ensured that the supercapacitor was within the safe operating temperature range, and strictly follows the charge/discharge criteria. The charging and discharging currents ranged from 10A to 100A to simulate

the fluctuating power of the supercapacitor. The final response time of the supercapacitor was 15ms at the shortest and 145s at the longest, and the response time of the lithium battery is 6 minutes at the shortest and 259 minutes at the longest.

According to wavelet packet decomposition, the optimal number of layers is $n = 8$, so $S_{(8,0)}$ is the objective function. The length of each frequency band is 1.857×10^{-3} Hz, so the $S_{(8,1)}$ frequency band is $[2.857 \times 10^{-3}, 3.605 \times 10^{-3}]$. By analogy, we can obtain the $S_{(8,4)}$ frequency band as $[1.657 \times 10^{-3}, 2.105 \times 10^{-3}]$ and the $S_{(8,16)}$ frequency band as $[1.924 \times 10^{-2}, 5.605 \times 10^{-2}]$.

Therefore, the low-, intermediate-, and high-frequency power distributions shown in Table 5 can be obtained. Some research, such as [30], setting 0.016Hz as the low and high frequency cut-off point, with signals above this frequency compensated by SC and below this frequency compensated by vanadium redox batteries. And [31] divides output power fluctuations into a high frequency region above 1 Hz, a medium frequency region between 0.01-1 Hz and a low frequency region below 0.01 Hz, where the medium-frequency region uses batteries and supercapacitors to build a hybrid energy storage system to smooth out power fluctuations and achieve a smooth grid connection. In this paper, as revealed by the photovoltaic power distribution method based on adaptive wavelet packet decomposition, lithium battery and supercapacitor absorb the intermediate frequency power and high frequency power of the original photovoltaic power generation respectively, whereas the low frequency signal is directly connected to the grid.

Table 5. Low-, intermediate- and high-frequency power distributions.

Frequency band type	Frequency (Hz)
Low frequency	$S_{(8,1)} - S_{(8,4)}$
Intermediate frequency	$S_{(8,4)} - S_{(8,16)}$
High frequency	$S_{(8,16)} - S_{(8,63)}$

4.3. Wavelet packet decomposition results of photoelectric power

The low-frequency power signal decomposed by the adaptive wavelet packet is shown in Figure 12.

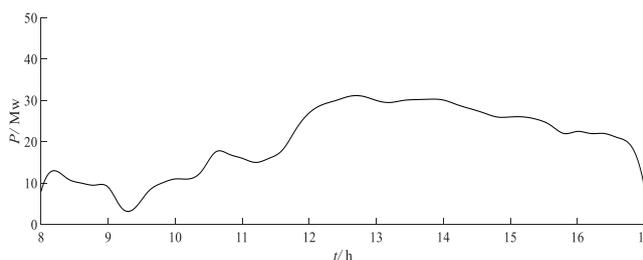


Figure 12. Low frequency power after the adaptive wavelet packet decomposition method.

The low-frequency component has large energy and small local fluctuation amplitude. It can be seen that the power fluctuation of the filtered low-frequency power part after improved wavelet packet decomposition satisfies the grid connection criteria, the low-frequency power P_0 can be directly connected to the grid.

The Figure 13 is the intermediate-frequency power of adaptive wavelet packet decomposition. Although the intermediate-frequency term has power fluctuations, the amplitude is not very large. Combined with the energy storage characteristics of the lithium battery, once the stabilization device is stabilized, this term is output to the lithium battery in the form of P_{Li} with the aim to store electric energy.

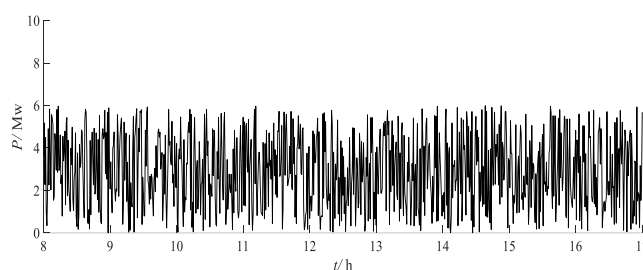


Figure 13. Intermediate-frequency power after the adaptive wavelet packet decomposition method.

The high frequency power signal after adaptive wavelet packet decomposition is shown in Figure 14. As shown in Figure 14, the high-frequency fraction of the original photoelectric power fluctuates significantly. When this fraction is directly connected to the system or supplied with energy storage batteries for storage, the safety of regional microgrid operation is affected. According to the characteristics of the supercapacitor, the high-frequency power is output to the supercapacitor unit designed herein as P_{sc} and combined with the coordinated control strategy designed to smooth the high-frequency signal of the photoelectric power.

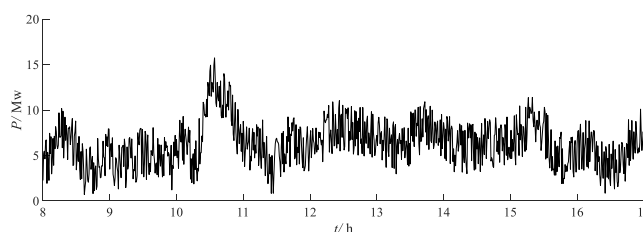


Figure 14. High-frequency power after the adaptive wavelet packet decomposition method.

Comparing to the conventional method, such as low-pass filtering and its related algorithms in [32-34], the resolution of high and low frequency power is low in these decomposition results due to the characteristics of the low-pass filter phase lag. And this issue does not exist in this paper. Also,

compared with the online wavelet filtering method used in [35], which reduces the phase delay in the low-pass filter, but leads to the problem of blurring the division between the high-frequency and low-frequency power components. The improved wavelet packet decomposition method used in this paper takes whether the grid connection condition is satisfied as the test criterion to determine the optimal number of decomposition layers, and results show the effectiveness of the proposed method.

4.4. Supercapacitor-lithium battery coordinated control strategy verification

After the improved wavelet packet decomposition, the decomposed medium and high frequency power are sent to the lithium batter and supercapacitor, respectively. This is widely accepted that delivering the fluctuating power components that require fast response to power-usage storage and the relatively stable power components to energy-usage storage can circumvent both defects and make the energy storage technology perfect [36-37].The high frequency component of the original photoelectric power after smoothing by the supercapacitor unit is shown in Figure 15.

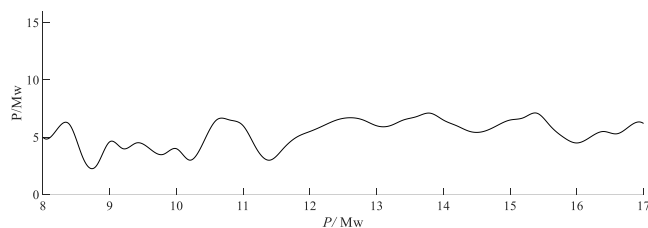


Figure 15. Smoothed high-frequency power component.

It is obviously seen that the local fluctuations of the output power after smoothing by the supercapacitor bank is significantly reduced compared to the original high-frequency power, which verifies that the proposed coordinated control strategy for supercapacitor bank can indeed reduce the high-frequency partial power fluctuations.

After that, we combined the control strategy of supercapacitors and lithium batteries as well as the charging-discharging states of the hybrid energy storage component. The half-physical simulation is used to obtain the actual photovoltaic connection to grid power P_v^* smoothed by the mixed energy storage system, as shown in Figure 16.

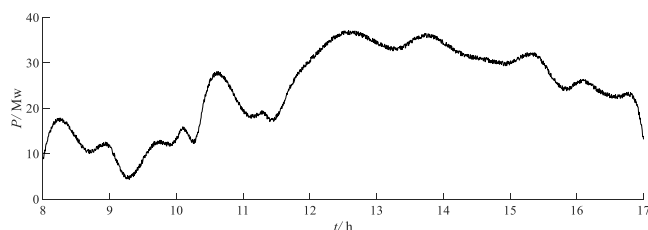


Figure 16. Actual grid connection curve of the photovoltaic power generation system.

According to the simulation results, once the hybrid energy storage device is introduced, the maximum power fluctuation of the large-capacity lithium battery power output during the sampling period and the average power fluctuation of the entire cycle were 3.12 and 2.61 MW, respectively. Compared with the power fluctuation before smoothing, smoothing reduced the power fluctuation by 26.7%, with the local fluctuation of the grid-connected power being significantly lower than that of the original power generation system.

5. CONCLUSIONS

Through semi-physical simulation analysis, we obtained the following conclusions. By combining the energy storage characteristics of supercapacitors and large-capacity lithium batteries, we developed a power distribution method based on adaptive wavelet packet decomposition. This method fully exploits the advantages of supercapacitors and lithium batteries. The SC-Li coordinated control strategy can effectively smooth the high frequency signal of the original photoelectric power. The hybrid energy storage device and control strategy designed herein smoothed the photovoltaic power generation, resulting in stable grid-connected power. The fluctuation range in the short term was significantly reduced, and the overall fluctuation range remained un-changed.

ACKNOWLEDGEMENTS

This paper was funded by Foundation of National Defense Science and Technology Key Laboratory, grant number 6142217200307.

References

1. B. Li, J. Zhang. *Sol. Energy*, 210 (2020) 68.
2. J. Antonanzas, N. Osorio, R. Escobar, R. Urraca, F.J. Martinez-de-Pison, F. Antonanzas-Torres. *Sol. Energy*, 136 (2016) 78.
3. Mellit, M. Pavan, Ogliari, Leva, Lugh. *Appl. Sci.*, 10 (2020) 487.
4. D. Van, J. Widén, J. Munkhammar. *Renewable Sustainable Energy Rev.*, 81 (2018) 1484.
5. M. Bragard, N. Soltau, S. Thomas, De Doncker, R.W.. *IEEE T. Power Electr.*, 25 (2010) 3049.
6. Y. Yu, G. Konstantinou, B. Hredzak, V. G. Agelidis. *IEEE T. Power Electr.*, 31 (2016) 292.
7. K. Doubleday, V. Hernandez, BM Hodge. *Sol. Energy*, 206 (2020) 52.
8. A. Arani, H. Karami, G. B. Gharehpetian, M. S. A. Hejazi. *Renewable Sustainable Energy Rev.*, 69 (2017) 9.
9. M. C. Argyrou, P. Christodoulides, S. A. Kalogirou. *Renewable Sustainable Energy Rev.*, 94 (2018) 804.
10. C. Tian, K. Li, Y. Yan, C. Zhang. *Power System Technology*, 39 (2015) 2167.
11. F. Liu, J. Liu, L. Zhou. A novel control strategy for hybrid energy storage system to relieve battery stress, *The 2nd International Symposium on Power Electronics for Distributed Generation Systems(PEDG)*, Hefei, China, 2010, 929.
12. C. Sandoval, V. M. Alvarado, J. C. Carmona, G. L. Lopez, J. F. Gomez-Aguilar. *Renewable Energy*, 105 (2017) 407.
13. J. Zou, B. Dai, C. Peng, X. Xin, W. Luo. *Automation of Electric Power Systems*, 37 (2013) 1.

14. X. Han, Y. Chen, H. Zhang, F. Chen. *Proceedings of the CSEE*, 33 (2013) 8.
15. X. Feng, J. Gu, X. Guan. *J. Mod. Power Syst. Clean Energy*, 6 (2018) 107.
16. A. Atif, M. Khalid. *IEEE Access*, 8 (2020) 33806.
17. M. C. Alexiadis, P. S. Dokopoulos. *IEEE T. Energy Convers.*, 14 (1999) 836.
18. F. Wu, J. Wang, Z. Sun, T. Wang, L. Chen, X. J. E. Han. *Energies*, 12 (2019) 4642.
19. K. Bi, L. Sun, Q. An, J. Duan. *IEEE T. Power Electr.*, 5 (2019) 4981.
20. S. Liu, L. Wei, H. Wang. *Appl. Energy*, 278 (2020) 115436.
21. W. Kai, R. Baosen, L. Liwei, L. Yuhao, Z. Hongwei, S. Zongqiang. A review of modeling research on supercapacitor, *2017 Chinese Automation Congress(CAC)*, Jinan, China, 2017, 5998.
22. M. E. Şahin, F. Blaabjerg, A. Sangwongwanich. *CPSS*, 6 (2021) 31.
23. C. Wang, H. He, Y. Zhang, H. Mu. *Appl. Energy*, 196 (2017) 268.
24. S. Bansal, P. Nambisan, P. Saha, M. Khanra. *J. Energy Storage*, 51 (2022) 104517.
25. C. Luan, D. S. Oliveira, F. Antunes, D. Alves, J. Souza. A soft switching bidirectional DC-DC converter based on three-state switching cell, *IEEE Annual Energy Conversion Congress and Exposition*, Baltimore, Maryland, USA, 2015, 4656.
26. P. Roy, J. He, Y. Liao. *IEEE Access*, 8 (2020) 2169.
27. J. Li, M. Ye, K. Gao, S. Jiao, J. Xu. *Ionics*, 27 (2021) 3909.
28. X. Dong, C. Zhang, J. Jiang. *Energy Procedia*, 152 (2018) 520.
29. W. Li, F. Duan, C. Xu. *IEEE Access*, 7 (2019) 31971.
30. X. Li, J. Wang, Y. Qiu, Y. Hou, Q. Zhou, *Taiyangneng Xuebao*, 43 (2022) 88.
31. J. Wu, M. Ding. *Automation of Electric Power Systems*, 41 (2017) 7.
32. S. K. Kollimalla, M. K. Mishra, A. Ukil, H. B. Gooi. *IEEE Trans. Sustain. Energy*, 8 (2017) 772.
33. A. Tani, M. B. Camara, B. Dakyo. *IEEE Trans. Ind. Appl.*, 51 (2015) 1817.
34. S. Kotra, M. K. Mishra. *IEEE Trans. Ind. Electron.*, 64 (2017) 3640.
35. S. N. Christian, K. Z. Liu. *Conference of the IEEE Industrial Electronics Society*. Florence, Italy, 2016, 2089.
36. W. Li, G. Joos, C. Abbey. Wind power impact on system frequency deviation and an ESS based power filtering algorithm solution, *IEEE PES Power Systems Conference and Exposition*, Atlanta, USA, 2016, 2077.
37. T. Guo T, Y. B. Liu, J. B. Zhao, Y. Zhu, J. Liu. *Int. J. Elec. Power*, 116 (2020) 105579.

© 2022 The Authors. Published by ESG (www.electrochemsci.org). This article is an open access article distributed under the terms and conditions of the Creative Commons Attribution license (<http://creativecommons.org/licenses/by/4.0/>).